J. Fluid Mech. (2026), *vol.* 1027, A26, doi:10.1017/jfm.2025.11096

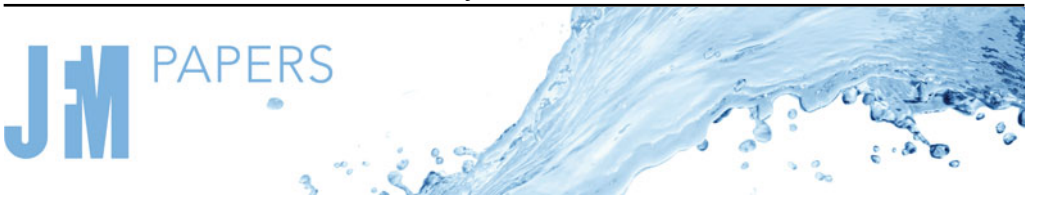

Scaling of wall pressure and the streamwise turbulence intensity peak in compressible wall flows

Asif Manzoor Hasan[1], **Pedro Costa**[1], **Johan Larsson**[2] **and Rene Pecnik**[1]

[1]Process & Energy Department, Delft University of Technology, Leeghwaterstraat 39, 2628 CB Delft, The Netherlands

[2]Department of Mechanical Engineering, University of Maryland, College Park MD, 20742, USA

Corresponding authors: Asif Manzoor Hasan, a.m.hasan@tudelft.nl; Rene Pecnik, r.pecnik@tudelft.nl

(Received 13 May 2025; revised 9 September 2025; accepted 2 December 2025)

This paper develops scaling laws for wall-pressure root mean square and the streamwise turbulence intensity peak, accounting for both variable-property and intrinsic compressibility effects – those associated with changes in fluid volume due to pressure variations. To develop such scaling laws, we express the target quantities as an expansion series in powers of an appropriately defined Mach number. The leading-order term is represented using the scaling relations developed for incompressible flows, but with an effective Reynolds number. Higher-order terms capture intrinsic compressibility effects and are modelled as constant coefficients, calibrated using flow cases specifically designed to isolate these effects. The resulting scaling relations are shown to be accurate for a wide range of turbulent channel flows and boundary layers.

Key words: compressible turbulence, turbulent boundary layers

1. Introduction

Wall-pressure fluctuations significantly impact the structural integrity of surfaces as well as the noise that they emit (Bull 1996). Their accurate prediction is vital for engineering applications, particularly in high-speed flows where such fluctuations become more intense and pose greater design challenges. As a result, the scaling behaviour of wall-pressure fluctuations in compressible flows has been an active area of research for several decades (Laganelli, Martellucci & Shaw 1983; Bernardini & Pirozzoli 2011; Ritos, Drikakis & Kokkinakis 2019; Zhang *et al.* 2022, 2024; Gerolymos & Vallet 2023).

Among the different Reynolds stresses, studying the scaling behaviour of the streamwise turbulence intensity peak has garnered the most attention in the incompressible flow community (see e.g. Marusic, Baars & Hutchins 2017; Chen & Sreenivasan 2021; Smits *et al.* 2021; Monkewitz 2022). However, in contrast to wall pressure, relatively few studies have examined the scaling of the peak intensity in compressible flows.

In incompressible flows, neither wall pressure nor the peak of streamwise turbulence intensity collapses under wall scaling (i.e. scaled using the friction velocity u_τ and the viscous length scale δ_v). Instead, these inner-scaled quantities increase with the friction Reynolds number Re_τ (Chen & Sreenivasan 2022). Recently, with high-Reynolds-number experimental and numerical data, various semi-empirical scaling laws have been proposed to capture this increase with Re_τ. There are particularly two schools of thought behind these scaling laws. One, according to Townsend's attached eddy model, advocates that the wall pressure and the peak streamwise turbulence intensity increase indefinitely as a logarithmic function of Re_τ (Marusic *et al.* 2017; Panton, Lee & Moser 2017; Smits *et al.* 2021). The other approach corresponds to the power-law theory developed by Chen & Sreenivasan (2021), which argues that at infinitely high Re_τ, both wall pressure and the peak intensity (among other quantities) should asymptote to a constant value. The power-law increase of the peak intensity was recently supported by the high-Reynolds-number pipe flow direct numerical simulations (DNS) ($Re_\tau \approx 12\,000$) of Pirozzoli (2024). While the debate between these two theories is still ongoing, the focus of this paper is to extend these scaling theories to variable-property and compressible flows, where other parameters such as the free-stream Mach number M_∞ and the wall cooling ratio T_w/T_r (where T_w and T_r correspond to the wall and adiabatic temperatures, respectively) also become important. (Note that other wall-cooling parameters – such as the diabatic parameter $\Theta = (T_w - T_\infty)/(T_r - T_\infty)$ (Zhang *et al.* 2014; Cogo *et al.* 2023), where T_∞ is the free-stream temperature, and the Eckert number $Ec = (\gamma - 1)M_\infty^2 T_\infty/(T_r - T_w)$ (Wenzel, Gibis & Kloker 2022) – have been found to be more effective in quantifying wall-cooling effects than T_w/T_r.)

Kistler & Chen (1963) performed the first measurement of wall-pressure fluctuations underneath supersonic boundary layers (free-stream Mach number $M_\infty \leqslant 5$), followed by other experimental studies summarised in figure 1 of Beresh *et al.* (2011). Based on such experimental datasets, Laganelli *et al.* (1983) developed an engineering model for wall-pressure root mean square (r.m.s.) scaled by the free-stream dynamic pressure ($q_\infty = 0.5\rho_\infty U_\infty^2$, where subscript ∞ implies free-stream values). The experimental measurements used to tune Laganelli's model were found to exhibit significant scatter, largely due to their high sensitivity to the measurement sensors (Beresh *et al.* 2011), thereby raising concerns about the model's accuracy. This high level of scatter also hindered the development of more accurate models (Beresh *et al.* 2011).

Bernardini & Pirozzoli (2011) reported some of the earliest wall-pressure r.m.s. data using DNS. They found that for their supersonic adiabatic boundary layers ($T_w/T_r = 1$), wall-pressure r.m.s. scaled by wall shear stress τ_w (i.e. $p^+_{w,rms}$) collapses for data at similar Re_τ. However, a strong Mach number effect was seen if $p_{w,rms}$ was scaled by q_∞, suggesting that τ_w better characterises wall-pressure. Similarly, Duan, Choudhari & Zhang (2016) observed a weak Mach number effect on $p^+_{w,rms}$ for their quasi-adiabatic ($T_w/T_r = 0.76$) boundary layer at hypersonic Mach number ($M_\infty = 5.86$). However, Zhang, Duan & Choudhari (2017) observed that at the same M_∞, $p^+_{w,rms}$ substantially increases when the wall is strongly cooled, i.e. $T_w/T_r = 0.25$. More recently, Zhang *et al.* (2022) observed that $p^+_{w,rms}$ decreases with wall cooling at subsonic and supersonic Mach numbers, but increases with wall cooling at hypersonic Mach numbers, $M_\infty > 5$. They subsequently retuned the constants in Laganelli's model to better fit their data. Even more recently,

Zhang *et al.* (2024) proposed another scaling model for $p^+_{w,rms}$ as a function of the free-stream Mach number for adiabatic boundary layers. However, this model does not account for changes in Re_τ and T_w/T_r.

As for boundary layers, several DNS studies were performed to study wall pressure and its scaling in fully developed channel flows. Yu, Xu & Pirozzoli (2020) decomposed the pressure field into rapid, slow, viscous and compressible parts, and observed that the compressible pressure increases strongly with the bulk Mach number. Later, Yu *et al.* (2022) observed that this increase is better characterised in terms of the friction Mach number $M_\tau = u_\tau/c_w$, where c_w is the speed of sound at the wall. More recently, Gerolymos & Vallet (2023), using their comprehensive dataset of compressible channel flows, proposed a scaling relation for $p^+_{w,rms}$ that can be applied to both channels and boundary layers.

The wall-pressure scaling laws proposed for boundary layers, such as the ones in Laganelli *et al.* (1983) and Zhang *et al.* (2024), have not been generalised to other classes of flows, such as channel and pipe flows. Moreover, the model of Gerolymos & Vallet (2023), which was originally tested for channel flows, leads to significant errors for high-Mach-number boundary layers. Clearly, a universally applicable and accurate scaling law is lacking.

Compared to wall-pressure fluctuations, less work has been done to study the scaling behaviour of the streamwise turbulence intensity peak in compressible flows. For variable-property channel flow cases at zero Mach number, Patel *et al.* (2015) observed that the peak of inner-scaled streamwise turbulence intensity can be higher or lower than a corresponding incompressible flow at similar Re_τ, depending on the distribution of the semi-local Reynolds number Re^*_τ (defined as $\bar{\rho}u^*_\tau\delta/\bar{\mu}$, where $\bar{\rho}$ and $\bar{\mu}$ are mean density and viscosity, $u^*_\tau = \sqrt{\tau_w/\bar{\rho}}$ is the semi-local friction velocity, and δ corresponds to the boundary layer thickness or the channel half-height). Specifically, the peak intensity is higher if Re^*_τ decreases away from the wall, and lower if it increases.

For flows at non-zero Mach numbers, the peak value is found to be higher than a corresponding incompressible flow at similar Re_τ, independent of the distribution of Re^*_τ (Gatski & Erlebacher 2002; Foysi, Sarkar & Friedrich 2004; Pirozzoli, Grasso & Gatski 2004; Duan, Beekman & Martin 2010; Modesti & Pirozzoli 2016; Zhang, Duan & Choudhari 2018; Trettel 2019; Cogo *et al.* 2022, 2023). In Hasan *et al.* (2025), it was concluded that the higher value of the peak is due to intrinsic compressibility effects – those associated with changes in fluid volume in response to changes in pressure (Lele 1994). However, a formal scaling law that accounts for these effects is missing.

In this paper, we develop scaling laws for wall-pressure r.m.s. and the streamwise turbulence intensity peak that account for compressibility effects – variable-property and intrinsic compressibility (Lele 1994; Hasan *et al.* 2025) – and are applicable to both channel/pipe flows and boundary layers. To develop such scaling laws, we express wall-pressure r.m.s. and the peak intensity as an expansion series in powers of an appropriately defined Mach number (Ristorcelli 1997). The leading-order term in this series accounts for Reynolds number and variable-property effects, and is represented by using the same scaling laws as developed for incompressible flows (Chen & Sreenivasan 2022), but with an effective value of the semi-local friction Reynolds number instead of the wall-based Re_τ. The higher-order terms mainly account for intrinsic compressibility effects, and are modelled using the constant-property high-Mach-number cases of Hasan *et al.* (2025), which are designed to isolate these effects.

2. Approach

For compressible homogeneous flows, Ristorcelli (1997) expressed quantities such as pressure, density and velocity in the form of expansion series as follows:

$$\begin{aligned} p'/\mathcal{P} &= \epsilon^2\left[p_1'/\left(\rho_\infty \mathcal{U}^2\right) + \epsilon^2\, p_2'/\left(\rho_\infty \mathcal{U}^2\right) + \epsilon^4\, p_3'/\left(\rho_\infty \mathcal{U}^2\right) + \cdots\right], \\ \rho'/\rho_\infty &= \epsilon^2\left[\rho_1'/\rho_\infty + \epsilon^2\, \rho_2'/\rho_\infty + \epsilon^4\, \rho_3'/\rho_\infty + \cdots\right], \\ u_i/\mathcal{U} &= u_{0i}/\mathcal{U} + \epsilon^2\left[u_{1i}/\mathcal{U} + \epsilon^2\, u_{2i}/\mathcal{U} + \epsilon^4\, u_{3i}/\mathcal{U} + \cdots\right], \end{aligned} \tag{2.1}$$

where $\mathcal{P}$ is the thermodynamic scale of pressure, $\mathcal{U}$ is the velocity scale, ρ_∞ is the reference background density, $\epsilon^2 = \rho_\infty \mathcal{U}^2/\mathcal{P}$ is the ratio of the hydrodynamic scale of pressure $\rho_\infty \mathcal{U}^2$ to the thermodynamic scale, and the subscripts 0, 1, 2, 3 signify the order of the variables. Here, the single prime denotes fluctuations from Reynolds average. When these expansions are substituted into the Navier–Stokes equations, and the terms with similar powers of ϵ are grouped, it produces a set of zeroth-order (proportional to ϵ^0), first-order (proportional to ϵ^2) and higher-order governing equations. The zeroth-order set of equations solves for the incompressible velocity u_{0i} and pressure p_1', whereas the higher-order equations solve for the higher order variables. (Note that since the pressure term in the Navier–Stokes equation, upon appropriate non-dimensionalisation, is multiplied with ϵ^{-2}, a first-order pressure p_1' acts as the incompressible pressure to satisfy a meaningful balance between velocity and pressure terms; Ristorcelli 1997.)

It is worth noting that in these expansions, Ristorcelli (1997) assumed the thermodynamic scale of pressure to be the reference background pressure P_∞, and the velocity scale to be $(2k/3)^{1/2}$, where k is the turbulent kinetic energy defined as $k = \overline{u_i' u_i'}/2$, with the overline denoting Reynolds averaging. This gives $\epsilon^2 = \rho_\infty (2k/3)/P_\infty$, which is equal to γM_t^2 for ideal gas flows, where γ is the ratio of specific heats, and $M_t = (2k/3)^{1/2}/c_\infty$, with c_∞ being the reference speed of sound.

Let us now extend Ristorcelli's approach to compressible wall-bounded flows, but with some notable differences. For homogeneous flows, Ristorcelli (1997) represented the compressible flow field as a sum of an incompressible field and higher-order fields, with the latter capturing effects that arise only at finite Mach numbers. In the same spirit, we represent a compressible wall-bounded flow field as a sum of a variable-property zero-Mach-number field – i.e. the flow field that would exist in a variable-property flow at zero Mach number with the same Reynolds number and mean property distributions as the compressible flow – and higher-order fields representative of finite-Mach-number effects. Such an expansion ensures that the zeroth-order term in the expansion series comprises variable-property and Reynolds number effects, such that the higher-order terms primarily represent intrinsic compressibility effects that occur only at finite Mach numbers.

Some other differences are as follows. Since the base (zeroth-order) state about which the expansion series is built represents a zero-Mach-number flow with mean property variations, the reference density ρ_∞ and c_∞ in Ristorcelli's work should be replaced with the local mean density $\bar{\rho}$ and the local mean speed of sound $\bar{c}$, respectively. Additionally, the semi-local friction velocity scale u_τ^* becomes the relevant scale in compressible wall-bounded flows, instead of $(2k/3)^{1/2}$. Finally, we choose the thermodynamic pressure scale to be $\bar{\rho}\bar{c}^2$ rather than $\bar{p}$, for the following reason. The isentropic density fluctuations are related to pressure fluctuations through the relation $(\rho')^{is}/\bar{\rho} \approx p'/(\bar{\rho}\bar{c}^2)$ (Hasan *et al.* 2025). This implies that the density fluctuations depend on $\bar{\rho}\bar{c}^2$. Since intrinsic compressibility effects are, by definition, related to isentropic density fluctuations, it is natural that the parameter characterising these effects – namely, ϵ – also depends on $\bar{\rho}\bar{c}^2$.

Taking $\mathcal{P} = \bar{\rho}\bar{c}^2$, along with $\bar{\rho}u_\tau^{*2}$ as the hydrodynamic pressure scale, we get

$$\epsilon^2 = \bar{\rho}u_\tau^{*2}/\left(\bar{\rho}\bar{c}^2\right) = M_\tau^{*2}. \tag{2.2}$$

By accounting for these differences, we get the expansion series for pressure fluctuations in wall-bounded flows (analogous to (2.1) for homogeneous flows) as

$$p'/\left(\bar{\rho}\bar{c}^2\right) = M_\tau^{*2}\left[p_1'/\left(\bar{\rho}u_\tau^{*2}\right) + M_\tau^{*2}\, p_2'/\left(\bar{\rho}u_\tau^{*2}\right) + M_\tau^{*4}\, p_3'/\left(\bar{\rho}u_\tau^{*2}\right) + \cdots\right]. \tag{2.3}$$

By writing this equation at the wall, squaring it, averaging, and dividing by M_τ^{*4}, we get the equation for wall-pressure variance, scaled by τ_w^2, as

$$\overline{p'p'}_w^{+} = \overline{p_1'p_1'}_w^{+} + M_\tau^{*2}\left[2\,\overline{p_1'p_2'}_w^{+} + M_\tau^{*2}\left(\overline{p_2'p_2'}_w^{+} + 2\overline{p_1'p_3'}_w^{+}\right) + \cdots\right], \tag{2.4}$$

where the first term on the right-hand side signifies wall-pressure variance in a zero-Mach-number variable-property flow.

At this point, it is important to note that not only the leading-order correlation, but also other higher-order correlations on the right-hand side are mainly influenced by Reynolds number and variable-property effects. This is justified as follows. From the analysis of Ristorcelli (1997), we note that the first-order equations – governing the evolution of first-order velocity, second-order density and second-order pressure (u_{i1}, ρ_2' and p_2') – depend explicitly on the leading-order (incompressible) variables: u_{i0}, ρ_1' and p_1'. For wall-bounded flows, this implies that these higher-order variables (u_{i1}, ρ_2', p_2') are indirectly affected by Reynolds number and variable-property effects, through their dependence on the incompressible solution. Similarly, even higher-order quantities, such as u_{i2}, ρ_3', p_3', are primarily influenced by these effects through their dependence on lower-order variables. These higher-order quantities are not explicitly affected by intrinsic compressibility effects since there is no Mach number or ϵ in the set of governing equations (Ristorcelli (1997); see equations (23)–(26) therein); instead, such effects are embedded in the parameter ϵ by which these variables are multiplied in the expansion series.

Given this understanding, we model the correlations in (2.4) as a sum of a constant and a function that depends on Reynolds number and variable-property effects, inspired from the relations proposed for incompressible flows (Chen & Sreenivasan 2022). For instance, $\overline{p_1'p_1'}_w^{+} = c_{0,p} + f_{0,p}$, where $c_{0,p}$ is a constant, $f_{0,p}$ is an unknown function, and the subscript 0, p signifies the leading-order term for pressure. Representing all other higher-order correlations also in a similar form, and substituting them in (2.4), we get

$$\overline{p'p'}_w^{+} = \underbrace{c_{0,p} + f_{0,p}}_{Re\ \&\ \mathrm{VP}} + \underbrace{M_\tau^{*2}c_{1,p} + M_\tau^{*4}c_{2,p} + \cdots}_{\mathrm{IC}} + \underbrace{M_\tau^{*2}f_{1,p} + M_\tau^{*4}f_{2,p} + \cdots}_{\text{coupling } Re,\ \mathrm{VP},\ \mathrm{IC}}, \tag{2.5}$$

where '*Re*' denotes contribution by Reynolds number effects, 'VP' means variable-property effects, and 'IC' means intrinsic compressibility effects. Here, the terms consisting of the product of a constant (c) and the Mach number represent IC effects, whereas the terms consisting of the product of a variable-property- and Reynolds-number-dependent function f and the Mach number represent the coupling between *Re*, VP and IC effects.

Here, we postulate that the coupling effects are small, and can be neglected. We test this hypothesis *a posteriori* based on the available data. From this simplification, we get

$$\overline{p'p'}_w^{+} \approx c_{0,p} + f_{0,p} + M_\tau^{*2}c_{1,p} + M_\tau^{*4}c_{2,p} + \cdots\,. \tag{2.6}$$

Following a similar approach for the inner-scaled peak streamwise turbulence intensity, namely, $\widetilde{u''u''}_p^{*} = \overline{\rho u''u''}_p/\tau_w$ (where a tilde represents Favre averaging, and the double

primes denote fluctuations from Favre average), we get

$$\widetilde{u''u''}_p^* \approx c_{0,u} + f_{0,u} + M_\tau^{*2} c_{1,u} + M_\tau^{*4} c_{2,u} + \cdots, \tag{2.7}$$

where $c_{0,u}$, $c_{1,u}$, and so on are constants, analogous to $c_{0,p}$, $c_{1,p}$ for wall-pressure above. Here, $c_{0,u} + f_{0,u}$ represents the leading-order correlation $\widetilde{u_0''u_0''}_p^*$.

Before proceeding, we note that for ideal gases, the semi-local friction Mach number is approximately uniform (Hasan *et al.* 2025). This also holds for the non-ideal gas cases analysed here (Sciacovelli, Cinnella & Gloerfelt 2017). Thus hereafter, we assume $M_\tau^* \approx M_\tau$.

In the following subsections, we will model the unknown functions $f_{0,p}$ and $f_{0,u}$, and determine the constants in (2.6) and (2.7).

2.1. *Variable-property effects*

Patel *et al.* (2015) showed that semi-locally scaled wall pressure and the peak streamwise intensity (along with other quantities) are similar for flows with similar distributions of Re_τ^*, independent of the distributions of $\bar{\rho}$ and $\bar{\mu}$. Through this, they confirmed that variable-property effects simply change the local Reynolds number of the flow, conjectured earlier in Morkovin (1962) and Spina, Smits & Robinson (1994). Consequently, a natural choice to model $\overline{p_1'p_1'}_w^+ = c_{0,p} + f_{0,p}$ and $\widetilde{u_0''u_0''}_p^* = c_{0,u} + f_{0,u}$ would be to use the scaling relations developed for incompressible flows (Chen & Sreenivasan 2022), with an effective value of Re_τ^*.

It is well established in the incompressible flow literature that the dominant contribution to wall pressure arises from the source terms in the buffer layer (Kim 1989; Kim & Hussain 1993). In light of this, we propose that Re_τ^* computed in the buffer layer, say at $y^* = 15$ (where y^* is the semi-local wall distance defined as $y^* = y/\delta_v^*$, with the semi-local viscous length scale $\delta_v^* = \bar{\mu}/(\bar{\rho}u_\tau^*)$), should be used for scaling wall pressure.

For the peak intensity, the choice is not as straightforward as it was for wall-pressure r.m.s. One obvious choice is to compute the Reynolds number at the peak location itself ($y^* \approx 15$). Another choice is to use the wall Re_τ. The motivation for the latter choice comes from the analysis of Bradshaw (1967), who argued that the increase in the peak intensity with Re_τ for incompressible flows is directly associated with the large-scale fluctuations in wall shear stress. This is also mathematically supported by the Taylor series expansion of $\overline{u'u'}^+$ at the wall (Chen & Sreenivasan 2021; Smits *et al.* 2021), where the leading-order term represents fluctuations in wall shear stress.

To assess the correct Reynolds number that accounts for variable-property effects on wall shear stress fluctuations, and hence the peak intensity, we analyse the low-Mach-number variable-property cases of Modesti & Pirozzoli (2024) described in table 1. These cases are essentially free of intrinsic compressibility effects, and therefore quantify variable-property effects. For these cases, we have computed the wall shear stress fluctuations using the interpolation technique in Smits *et al.* (2021), and we observed that these fluctuations scale with Re_τ, and approximately follow the relation in Chen & Sreenivasan (2021), i.e. $0.25 - 0.42\,Re_\tau^{-1/4}$ (not shown). Following the discussion presented above, this implies that the peak intensity should also scale with Re_τ. This is verified in figure 1, which shows the semi-locally scaled peak intensity $\widetilde{u''u''}_p^*$ as a function of Re_τ and Re_τ^* taken at the peak location, i.e. $Re_\tau^*(y^* = 15)$. Clearly, the spread in the data with respect to the fit from Chen & Sreenivasan (2022) is lower for Re_τ than

Source	Type	Re_τ	M_∞, M_b	M_τ	T_w/T_r	Sym.
Boundary layer						
Bernardini & Pirozzoli (2011)	Conv.	403−1113	2−4	0.065−0.105	1	☆×8
Zhang *et al.* (2018)	Conv.	510, 646	2.5, 13.64	0.085, 0.195	0.18, 1	✚×2
Ceci *et al.* (2022)	Conv.	600−1000	5.84	0.149−0.161	0.25	◇×5
Huang *et al.* (2022)	Conv.	774, 1172	10.9	0.167, 0.182	0.2	✚×2
Cogo *et al.* (2022)	Conv.	453, 1947	2, 5.86	0.066−0.132	0.76	✖×4
Cogo *et al.* (2023)	Conv.	443	2−6	0.075−0.159	0.35−1	✖×12
A. Ceci (Private communication)	Conv.	450, 475	5.84, 7.87	0.130, 0.152	0.48, 0.76	△×2
Channel						
Trettel & Larsson (2016)	Conv.	437−1876	0.7−3	0.036−0.102	—	▽×6
Sciacovelli *et al.* (2017)	DG	402−692	1.5−3	0.08–0.15	—	▲×4
Modesti & Pirozzoli (2024)	LM	356−3203	≈0	≈0	—	△×13
Hasan *et al.* (2025)	CP	544−557	0.3−4	0.016–0.197	—	★×4

Table 1. Description of the 35 boundary layer and 27 channel flow cases used in this paper. Here, $Re_\tau = \rho_w u_\tau \delta/\mu_w$ is the friction Reynolds number based on the boundary layer thickness (δ) or the channel half-height (h), $M_\infty = U_\infty/c_\infty$ is the free-stream Mach number (for boundary layers), $M_b = U_b/c_w$ is the bulk Mach number (for channels), and $M_\tau = u_\tau/c_w$ is the wall friction Mach number, U_∞, U_b and u_τ denote the free-stream, bulk and friction velocities, respectively, c_∞ and c_w denote the speed of sound in the free-stream and at the wall, respectively, T_w/T_r is the wall-cooling parameter, with T_r being the adiabatic temperature. 'Conv.' indicates the conventional ideal gas cases, while 'DG' refers to the dense gas (supercritical) cases. Also, 'LM' denotes the low-Mach-number variable-property cases, in which mean property variations are induced by adding volumetric heat sources to the energy equation. Because these cases have very low Mach numbers, they are unaffected by intrinsic compressibility effects, thereby isolating variable-property effects. Finally, 'CP' represents constant-property high-Mach-number cases, where viscous-heating-induced mean property variations are balanced by volumetric heat sources such that the mean properties remain approximately constant throughout the domain. These cases thus isolate intrinsic compressibility effects. Finally, note that low-Reynolds-number cases in which Re_τ^* drops below 300 anywhere in the domain are excluded.

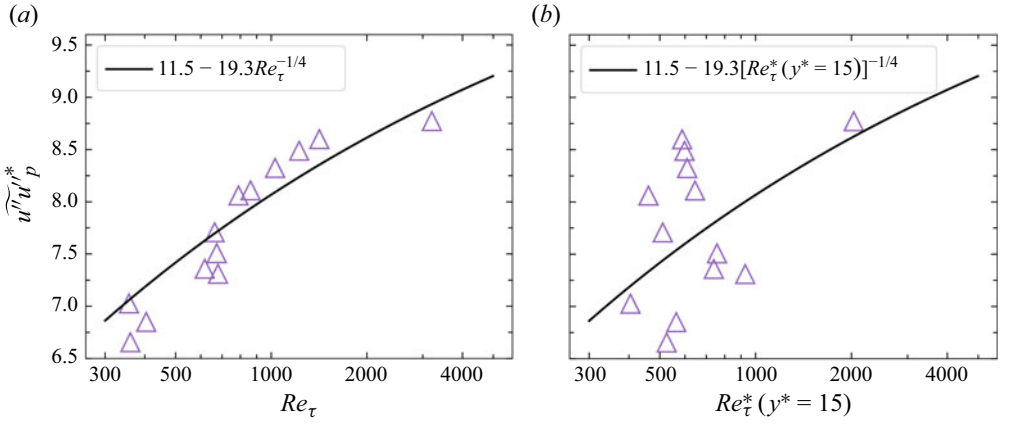

Figure 1. Semi-locally scaled streamwise turbulent peak intensity, i.e. $\widetilde{u''u''}_p^* = \overline{\rho u''u''}_p/\tau_w$ as a function of (*a*) Re_τ and (*b*) Re_τ^* taken at the peak location ($y^* = 15$), for the low-Mach-number variable-property cases of Modesti & Pirozzoli (2024). The black curve corresponds to the fit proposed in Chen & Sreenivasan (2022) for incompressible flows.

Quantity ϕ	$c_{0,\phi}$	$f_{0,\phi}$	$c_{1,\phi}$	$c_{2,\phi}$
Channels and pipes				
$\overline{p'p'}^{+}_{w}$	19.36	$-92.4[Re^{*}_{\tau}(y^{*}=15)]^{-1/4}+110.25[Re^{*}_{\tau}(y^{*}=15)]^{-1/2}$	2.4	8312.5
$\widetilde{u''u''}^{*}_{p}$	11.5	$-19.3\,Re_{\tau}^{-1/4}$	78.9	199.3
Boundary layers				
$\overline{p'p'}^{+}_{w}$	20.25	$-87.3[Re^{*}_{\tau}(y^{*}=15)]^{-1/4}+94.09[Re^{*}_{\tau}(y^{*}=15)]^{-1/2}$	2.4	8312.5
$\widetilde{u''u''}^{*}_{p}$	11.5	$-19.3\,Re_{\tau}^{-1/4}$	78.9	199.3

Table 2. The constants and functions in (2.6) and (2.7), i.e. $\phi = c_{0,\phi} + f_{0,\phi} + c_{1,\phi}M_{\tau}^{2} + c_{2,\phi}M_{\tau}^{4}$ (neglecting higher-order terms). The constant $c_{0,\phi}$ and the function $f_{0,\phi}$ are taken from Chen & Sreenivasan (2022), as discussed in § 2.1. The constants $c_{1,\phi}$ and $c_{2,\phi}$ are calibrated based on the constant-property high-Mach-number cases (Hasan *et al.* 2025), as discussed in § 2.2.

for $Re^{*}_{\tau}(y^{*}=15)$. Note that since these cases are at negligible Mach numbers, their peak intensity is a direct measure of the leading-order term in the expansion series, i.e. $\widetilde{u''_0u''_0}^{*}_{p}$.

Even though Re_{τ} is a better choice than the Reynolds number at the peak location, there is still some spread in the data around the curve fit (see figure 1*a*). This spread is mainly attributed to the effects associated with the gradients in the semi-local Reynolds number (Patel *et al.* 2015), which will be neglected here.

Finally, with these choices of the Reynolds numbers, we model the leading-order terms in (2.6) and (2.7) as described in table 2.

2.2. *Intrinsic compressibility effects*

We now determine the higher-order constants in (2.6) and (2.7) using the constant-property high-Mach-number cases of Hasan *et al.* (2025), designed to isolate intrinsic compressibility effects (see table 1).

Let us first focus on wall-pressure r.m.s. To obtain the constants, we first subtract the variable-property contribution $c_{0,\phi} + f_{0,\phi}$ (see table 2) from the total $\overline{p'p'}^{+}_{w}$ taken from the DNS. Next, we plot this difference – which signifies the contribution by intrinsic compressibility effects – as a function of the expansion parameter $\epsilon = M_{\tau}$ in figure 2(*a*) for the four constant-property cases (denoted by red stars). Fitting a curve of the form $M_{\tau}^{2}c_{1,p} + M_{\tau}^{4}c_{2,p}$ (neglecting higher-order terms) to these cases, we obtain $c_{1,p} = 2.4$ and $c_{2,p} = 8312.5$; see the black curve in figure 2(*a*).

Figure 2(*a*) also plots the intrinsic compressibility contribution for several boundary layer and channel flow cases in the literature, as listed in table 1. Despite the fact that these cases are at different Reynolds numbers, and possess different distributions of mean properties, a majority of the cases follow the curve fit set by the constant-property cases quite well. This corroborates the assumption that we made regarding neglecting the coupling terms earlier in this section.

However, there are some exceptions. First, for the boundary layer cases of Huang, Duan & Choudhari (2022), represented by a green plus, the deviation from the curve fit is quite high. This could be due to the simplifications that we made in the analysis. It is also possible that the intrinsic compressibility contribution to wall-pressure r.m.s. differs in boundary layers compared to channels. Thus the coefficients ($c_{1,p}$ and $c_{2,p}$) tuned based on the constant-property channels might not be accurate for boundary layers. Refining these coefficients for boundary layers would require constant-property high-Mach-number boundary layer simulations, which is deferred to future work. Nevertheless, in figure 2(*a*),

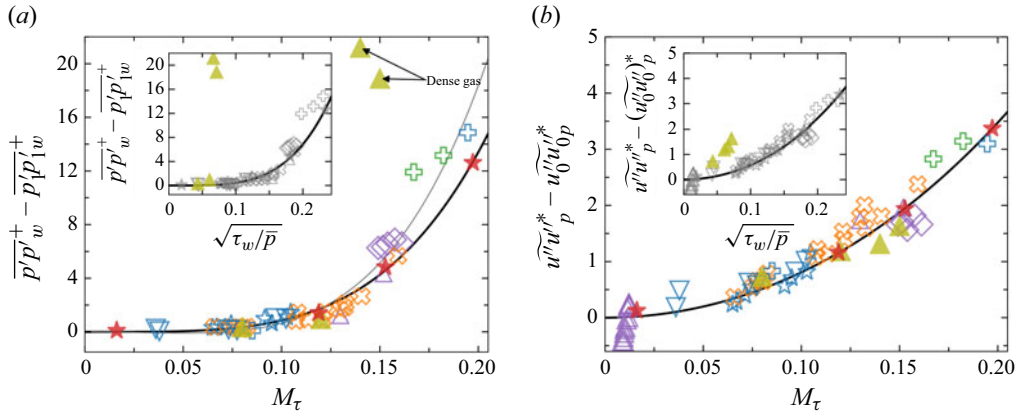

Figure 2. Contribution by intrinsic compressibility effects to (*a*) wall-pressure variance and (*b*) the peak streamwise turbulence intensity as a function of M_τ for a wide range of channels and boundary layers described in table 1. The black curves in (*a*) and (*b*) correspond to $c_{1,\phi}M_\tau^2 + c_{2,\phi}M_\tau^4$, where $c_{1,\phi}$ and $c_{2,\phi}$ are reported in table 2, and ϕ represents wall-pressure r.m.s. or the peak intensity. These coefficients are calibrated using the constant-property cases in table 1 (red stars). The grey curve in (*a*) corresponds to $c_{1,p}M_\tau^2 + c_{2,p}M_\tau^4$, where the coefficients $c_{1,p} = -66.9$ and $c_{2,p} = 13148.7$ are obtained using the turbulent boundary layer cases listed in table 1. The insets show the intrinsic compressibility contribution as a function of $\sqrt{\tau_w/\bar{p}}$. The grey symbols signify ideal gas air cases for which $\sqrt{\tau_w/\bar{p}} = \sqrt{1.4}M_\tau$, and the coloured symbols represent the dense gas cases of Sciacovelli *et al.* (2017).

we show the grey curve obtained using the conventional turbulent boundary layer cases listed in table 1. As expected, this curve aligns more closely with the green plus symbols.

Second, the dense gas cases of Sciacovelli *et al.* (2017) at high Mach numbers depict extremely high wall-pressure fluctuations. This is due to the proximity of these cases to the Widom line (the curve that marks the maximum of the specific heat at constant pressure, above the critical point). In this region, small pressure fluctuations can cause large density fluctuations, which in turn intensify pressure fluctuations through the source terms. Such an effect is due to the complexity of the equation of state, and is thus not accounted for in the present scaling model.

Repeating the same analysis for the peak of streamwise turbulence intensity, we get $c_{1,u} = 78.9$ and $c_{2,u} = 199.3$. Figure 2(*b*) shows the intrinsic compressibility contribution towards the peak intensity for the constant- and variable-property cases listed in table 1, along with the curve fit with tuned constants. Clearly, a majority of the cases follow the curve, corroborating that the coupling effects are small.

The insets in figure 2 show the intrinsic compressibility contributions to the wall-pressure r.m.s. and the peak intensity as functions of $\sqrt{\tau_w/\bar{p}}$ – the form that ϵ would take if $\bar{p}$ were chosen as the thermodynamic pressure scale. For the ideal gas air cases (shown in grey symbols), $\sqrt{\tau_w/\bar{p}}$ quantifies intrinsic compressibility effects as effectively as M_τ (main figure 2, discussed earlier), since $\sqrt{\tau_w/\bar{p}} \approx \gamma M_\tau$, with $\gamma = 1.4$ for these cases. However, for the dense gas cases of Sciacovelli *et al.* (2017) (shown in coloured symbols), the characterisation of intrinsic compressibility effects deteriorates for both wall pressure and the peak when $\sqrt{\tau_w/\bar{p}}$ is used instead of M_τ. These observations support our choice made in this section of using $\bar{\rho}\bar{c}^2$ as the relevant thermodynamic scale of pressure rather than $\bar{p}$. This is further supported by the observation that for the dense gas cases, the upward shift in the logarithmic mean velocity profiles due to intrinsic compressibility effects (Hasan *et al.* 2023) is well quantified in terms of M_τ, instead of $\sqrt{\tau_w/\bar{p}}$ (not shown).

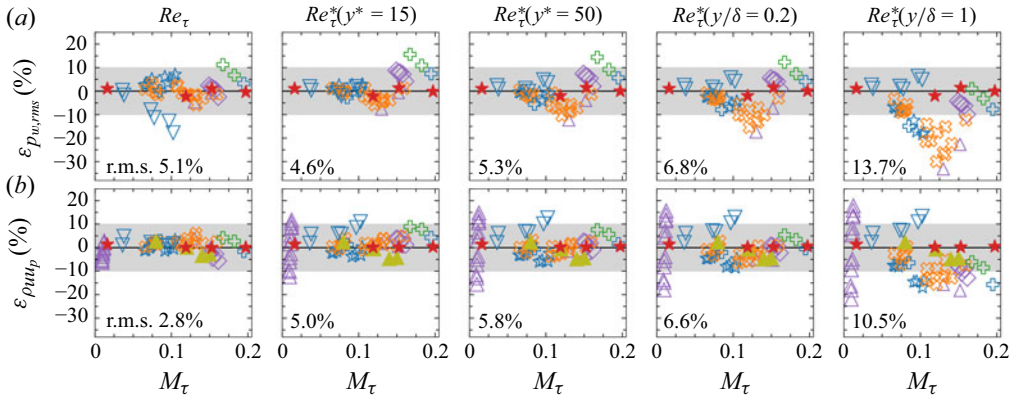

Figure 3. The error in the estimation of (*a*) wall-pressure r.m.s. and (*b*) the peak of streamwise turbulence intensity as a function of M_τ for the cases described in table 1. The errors are computed as discussed in the text. The different columns correspond to different Reynolds number definitions used while computing $f_{0,\phi}$ in table 2. The shaded areas represent an error margin of $\pm 10\,\%$.

Finally, it is interesting to note that for wall pressure, most of the intrinsic compressibility contribution comes from the quartic term $M_\tau^4 c_{2,p}$, while the same for the peak intensity stems from the quadratic term $M_\tau^2 c_{1,u}$. This is evident in figure 2, where the fitted curve appears quartic in figure 2(*a*) and quadratic in figure 2(*b*).

For wall pressure, the increase with Mach number has been attributed to the presence of travelling wave-packet-like structures in the pressure field (Yu *et al.* 2022; Zhang *et al.* 2022). These structures have been extensively studied in the literature (Yu, Xu & Pirozzoli 2019; Tang *et al.* 2020; Gerolymos & Vallet 2023; Yu *et al.* 2024), although the physical mechanism underlying their genesis is still unclear. Recently, Hasan *et al.* (2025) reported that the component of dilatational velocity (also termed non-pseudo-sound) associated with these wave-packet-like structures increases with $M_\tau^{3.3}$, close to a quartic dependence. This likely explains the quartic increase in wall pressure observed in figure 2(*a*).

For the streamwise turbulence intensity, our recent study (Hasan *et al.* 2025) concluded that the peak value increases due to the opposition of vortical motions by near-wall dilatational velocities. Specifically, this interaction modifies the turbulent shear stress, which in turn affects the production of streamwise turbulence intensity, thereby altering its peak value. This opposition mechanism scales with M_τ^2, thereby explaining the quadratic increase in the peak intensity.

3. The final scaling relations

By combining the functions and constants obtained from §§ 2.1 and 2.2, we get the final scaling relations for the wall-pressure r.m.s. and the peak streamwise turbulence intensity, as reported in table 2. Using these relations, we compute errors with respect to the DNS as $\varepsilon_\phi = (\phi^{DNS} - \phi^{model})/\phi^{DNS}$, where ϕ represents the wall-pressure r.m.s. or the peak intensity. We also compute the r.m.s. error across all cases as $\text{r.m.s.} = \sqrt{(1/N)\sum \varepsilon_\phi^2}$, where N is the total number of cases.

To demonstrate the accuracy of our scaling relations and the appropriateness of the Reynolds number choices described in § 2.1, figure 3 presents ε_ϕ for the wall-pressure r.m.s. (figure 3*a*) and the peak streamwise turbulence intensity (figure 3*b*), for the cases listed in table 1. Note that the densegas cases were excluded from the wall-pressure error

	Laganelli *et al.* (1983)†	Ritos *et al.* (2019)†	Zhang *et al.* (2022)†	Gerolymos & Vallet (2023)‡	Zhang *et al.* (2024)†	Present⋆
Max absolute error (%)	39	34.3	41.9	15.7	18.3	15.6
r.m.s. (%)	29	12.4	13.3	6.9	9.5	4.6

Table 3. The maximum absolute error (L_∞ norm) and the r.m.s. error (L_2 norm, defined in the main text) for various wall-pressure r.m.s. models available in the literature. The models marked with † have been applied exclusively to conventional (ideal gas air) boundary layers, for which they were originally developed. The model marked with ‡ has been tested on both conventional channels and boundary layers. Finally, the present model, marked by ⋆, has been applied to a broader set of flows, including conventional channels and boundary layers, as well as the four constant-property cases reported in Hasan *et al.* (2025).

calculations. The different columns correspond to different Reynolds number definitions used while computing $f_{0,\phi}$ in table 2. Clearly, the errors associated with the Reynolds number choices made in § 2.1 – namely, $Re^*_\tau(y^* = 15)$ for wall-pressure fluctuations, and Re_τ for the peak intensity – are relatively low when compared to those from other Reynolds number definitions, on average across all cases (compare their r.m.s. values). Furthermore, with these Reynolds number choices, a majority of the cases lie within the ± 10 % error band.

3.1. *Comparison with existing models*

Table 3 reports the maximum absolute error and the r.m.s. error in predicting the wall-pressure r.m.s. using various models from the literature. The errors reported in table 3 were computed by applying each model to the type of flow (channel or boundary layer) for which it was originally developed. For example, the models by Laganelli *et al.* (1983), Ritos *et al.* (2019) and Zhang *et al.* (2022, 2024) were applied exclusively to conventional air-like boundary layers. In contrast, the model by Gerolymos & Vallet (2023) was applied to both conventional channels and boundary layers, as listed in table 1. The present model was tested on a broader set of flows, including conventional channels and boundary layers, as well as the four constant-property cases reported in table 1.

As seen, the Laganelli family of models (Laganelli *et al.* 1983; Ritos *et al.* 2019; Zhang *et al.* 2022) yields relatively high error values, with r.m.s. error exceeding 12 %. The model proposed by Zhang *et al.* (2024) achieves a better accuracy, with r.m.s. error 9.5 %, despite not explicitly accounting for Reynolds number or wall-cooling effects. Among the models available in the literature, the best performance is observed for the model by Gerolymos & Vallet (2023), which achieves r.m.s. error 6.9 %. However, this value is still high, primarily due to significant errors incurred in predicting high-Mach-number boundary layers. The present model shows improved performance over existing approaches, with the lowest r.m.s. error 4.6 %.

Finally, for the streamwise turbulence intensity peak, using the proposed relation results in maximum absolute error 6.8 % and r.m.s. error 2.8 %. These values could not be compared to those obtained from other models in the literature as, to the best of our knowledge, there are currently no models available that predict this quantity in compressible flows.

4. Summary

In this paper, we have proposed scaling relations for the wall-pressure root mean square (r.m.s.) and the streamwise turbulence intensity peak, and tested them across a wide

range of turbulent channel and boundary layer cases from the literature. These relations were developed by expressing these quantities as an expansion series in terms of the friction Mach number M_τ. The first term in this series accounts for Reynolds number and variable-property effects, whereas the higher-order terms primarily capture intrinsic compressibility effects.

To model the leading-order term, we used the same expressions as proposed for incompressible flows, with an effective value of the semi-local Reynolds number that incorporates variable-property effects. For wall-pressure r.m.s, this value was found to be the Reynolds number defined in the buffer layer (at $y^* = 15$), whereas for the peak streamwise intensity, we found the effective value to be the wall Re_τ.

We model the higher-order correlations in the series as constants, whose values are found based on our constant-property high-Mach-number cases representative of intrinsic compressibility effects (Hasan *et al.* 2025). Modelling these correlations as simple constants implies that any coupling between Reynolds number, variable-property and intrinsic compressibility effects is small – an assumption that was verified *a posteriori* using the available data.

Finally, an additional key finding has been noted: based on the dense gas (non-ideal) cases of Sciacovelli *et al.* (2017), we confirm that $\bar{\rho}\bar{c}^2$ is a more appropriate thermodynamic pressure scale than the mean pressure $\bar{p}$, supporting the choice of expressing the expansion series in terms of M_τ.

We recommend the following for future work. (i) The proposed scaling approach should be tested for other turbulence quantities. (ii) The coupling effects neglected here should be explicitly quantified using a novel set of cases. For instance, to study the coupling between Reynolds number and intrinsic compressibility effects, one could simulate a similar set of constant-property, high-Mach-number cases as in Hasan *et al.* (2025), but at varying Reynolds numbers. Similarly, to study the coupling between variable-property and intrinsic compressibility effects, one could simulate cases with matching Reynolds numbers and mean property distributions but at varying Mach numbers (Lele 1994). (iii) Constant-property, high-Mach-number compressible boundary layers should be simulated to investigate how the intrinsic compressibility contribution to wall-pressure r.m.s. differs from that in channel flows. This could shed more light on why the curve in figure 2(*a*), fitted based on channels, is not quite accurate for some boundary layers.

Acknowledgements. We thank S. Pirozzoli (University of Rome) for insightful discussions.

Funding. This work was supported by European Research Council grant no. ERC-2019-CoG-864660, Critical, and the Air Force Office of Scientific Research under grant FA9550-23-1-0228.

Declaration of interests. The authors report no conflict of interest.

References

Beresh, S.J., Henfling, J.F., Spillers, R.W. & Pruett, B.O.M. 2011 Fluctuating wall pressures measured beneath a supersonic turbulent boundary layer. *Phys. Fluids* **23** (7), 075110.

Bernardini, M. & Pirozzoli, S. 2011 Wall pressure fluctuations beneath supersonic turbulent boundary layers. *Phys. Fluids* **23** (8), 085102.

Bradshaw, P. 1967 'Inactive' motion and pressure fluctuations in turbulent boundary layers. *J. Fluid Mech.* **30** (2), 241–258.

Bull, M.K. 1996 Wall-pressure fluctuations beneath turbulent boundary layers: some reflections on forty years of research. *J. Sound Vib.* **190** (3), 299–315.

Ceci, A., Palumbo, A., Larsson, J. & Pirozzoli, S. 2022 Numerical tripping of high-speed turbulent boundary layers. *Theor. Comput. Fluid Dyn.* **36** (6), 865–886.

Chen, X. & Sreenivasan, K.R. 2021 Reynolds number scaling of the peak turbulence intensity in wall flows. *J. Fluid Mech.* **908**, R3.

CHEN, X. & SREENIVASAN, K.R. 2022 Law of bounded dissipation and its consequences in turbulent wall flows. *J. Fluid Mech.* **933**, A20.
COGO, M., BAÙ, U., CHINAPPI, M., BERNARDINI, M. & PICANO, F. 2023 Assessment of heat transfer and Mach number effects on high-speed turbulent boundary layers. *J. Fluid Mech.* **974**, A10.
COGO, M., SALVADORE, F., PICANO, F. & BERNARDINI, M. 2022 Direct numerical simulation of supersonic and hypersonic turbulent boundary layers at moderate–high Reynolds numbers and isothermal wall condition. *J. Fluid Mech.* **945**, A30.
DUAN, L., BEEKMAN, I. & MARTIN, M.P. 2010 Direct numerical simulation of hypersonic turbulent boundary layers. Part 2. Effect of wall temperature. *J. Fluid Mech.* **655**, 419–445.
DUAN, L., CHOUDHARI, M.M. & ZHANG, C. 2016 Pressure fluctuations induced by a hypersonic turbulent boundary layer. *J. Fluid Mech.* **804**, 578–607.
FOYSI, H., SARKAR, S. & FRIEDRICH, R. 2004 Compressibility effects and turbulence scalings in supersonic channel flow. *J. Fluid Mech.* **509**, 207–216.
GATSKI, T.B. & ERLEBACHER, G. 2002 Numerical simulation of a spatially evolving supersonic turbulent boundary layer. *Tech. Rep.* NAS 1.15:211934. NASA.
GEROLYMOS, G.A. & VALLET, I. 2023 Scaling of pressure fluctuations in compressible turbulent plane channel flow. *J. Fluid Mech.* **958**, A19.
HASAN, A.M., COSTA, P., LARSSON, J., PIROZZOLI, S. & PECNIK, R. 2025 Intrinsic compressibility effects in near-wall turbulence. *J. Fluid Mech.* **1006**, A14.
HASAN, A.M., LARSSON, J., PIROZZOLI, S. & PECNIK, R. 2023 Incorporating intrinsic compressibility effects in velocity transformations for wall-bounded turbulent flows. *Phys. Rev. Fluids* **8** (11), L112601.
HUANG, J., DUAN, L. & CHOUDHARI, M.M. 2022 Direct numerical simulation of hypersonic turbulent boundary layers: effect of spatial evolution and Reynolds number. *J. Fluid Mech.* **937**, A3.
KIM, J. 1989 On the structure of pressure fluctuations in simulated turbulent channel flow. *J. Fluid Mech.* **205**, 421–451.
KIM, J. & HUSSAIN, F. 1993 Propagation velocity of perturbations in turbulent channel flow. *Phys. Fluids A: Fluid Dyn.* **5** (3), 695–706.
KISTLER, A.L. & CHEN, W.S. 1963 The fluctuating pressure field in a supersonic turbulent boundary layer. *J. Fluid Mech.* **16** (1), 41–64.
LAGANELLI, A.L., MARTELLUCCI, A. & SHAW, L.L. 1983 Wall pressure fluctuations in attached boundary-layer flow. *AIAA J.* **21** (4), 495–502.
LELE, S.K. 1994 Compressibility effects on turbulence. *Annu. Rev. Fluid Mech.* **26** (1), 211–254.
MARUSIC, I., BAARS, W.J. & HUTCHINS, N. 2017 Scaling of the streamwise turbulence intensity in the context of inner–outer interactions in wall turbulence. *Phys. Rev. Fluids* **2** (10), 100502.
MODESTI, D. & PIROZZOLI, S. 2016 Reynolds and Mach number effects in compressible turbulent channel flow. *Intl J. Heat Fluid Flow* **59**, 33–49.
MODESTI, D. & PIROZZOLI, S. 2024 Friction and heat transfer in forced air convection with variable physical properties. *J. Fluid Mech.* **1001**, A27.
MONKEWITZ, P.A. 2022 Asymptotics of streamwise Reynolds stress in wall turbulence. *J. Fluid Mech.* **931**, A18.
MORKOVIN, M.V. 1962 Effects of compressibility on turbulent flows. *Mécanique de la Turb.* **367** (380), 26.
PANTON, R.L., LEE, M. & MOSER, R.D. 2017 Correlation of pressure fluctuations in turbulent wall layers. *Phys. Rev. Fluids* **2** (9), 094604.
PATEL, A., PEETERS, J.W.R., BOERSMA, B.J. & PECNIK, R. 2015 Semi-local scaling and turbulence modulation in variable property turbulent channel flows. *Phys. Fluids* **27** (9), 095101.
PIROZZOLI, S. 2024 On the streamwise velocity variance in the near-wall region of turbulent flows. *J. Fluid Mech.* **989**, A5.
PIROZZOLI, S., GRASSO, F. & GATSKI, T.B. 2004 Direct numerical simulation and analysis of a spatially evolving supersonic turbulent boundary layer at $M = 2.25$. *Phys. Fluids* **16** (3), 530–545.
RISTORCELLI, J.R. 1997 A pseudo-sound constitutive relationship for the dilatational covariances in compressible turbulence. *J. Fluid Mech.* **347**, 37–70.
RITOS, K., DRIKAKIS, D. & KOKKINAKIS, I.W. 2019 Acoustic loading beneath hypersonic transitional and turbulent boundary layers. *J. Sound Vib.* **441**, 50–62.
SCIACOVELLI, L., CINNELLA, P. & GLOERFELT, X. 2017 Direct numerical simulations of supersonic turbulent channel flows of dense gases. *J. Fluid Mech.* **821**, 153–199.
SMITS, A.J., HULTMARK, M., LEE, M., PIROZZOLI, S. & WU, X. 2021 Reynolds stress scaling in the near-wall region of wall-bounded flows. *J. Fluid Mech.* **926**.
SPINA, E.F., SMITS, A.J. & ROBINSON, S.K. 1994 The physics of supersonic turbulent boundary layers. *Annu. Rev. Fluid Mech.* **26** (1), 287–319.

TANG, J., ZHAO, Z., WAN, Z.-H. & LIU, N.-S. 2020 On the near-wall structures and statistics of fluctuating pressure in compressible turbulent channel flows. *Phys. Fluids* **32** (11), 115121.
TRETTEL, A. & LARSSON, J. 2016 Mean velocity scaling for compressible wall turbulence with heat transfer. *Phys. Fluids* **28** (2), 026102.
TRETTEL, A.J. 2019 Transformations for variable-property turbulent boundary layers. PhD thesis, UCLA.
WENZEL, C., GIBIS, T. & KLOKER, M. 2022 About the influences of compressibility, heat transfer and pressure gradients in compressible turbulent boundary layers. *J. Fluid Mech.* **930**, A1.
YU, M., LIU, P., FU, Y., TANG, Z. & YUAN, X. 2022 Wall shear stress, pressure, and heat flux fluctuations in compressible wall-bounded turbulence, Part I: One-point statistics. *Phys. Fluids* **34** (6), 065139.
YU, M., XU, C.-X. & PIROZZOLI, S. 2019 Genuine compressibility effects in wall-bounded turbulence. *Phys. Rev. Fluids* **4** (12), 123402.
YU, M., XU, C.-X. & PIROZZOLI, S. 2020 Compressibility effects on pressure fluctuation in compressible turbulent channel flows. *Phys. Rev. Fluids* **5** (11), 113401.
YU, M., ZHOU, Z., DONG, S., YUAN, X. & XU, C. 2024 On the generation of near-wall dilatational motions in hypersonic turbulent boundary layers. *J. Fluid Mech.* **984**, A44.
ZHANG, C., DUAN, L. & CHOUDHARI, M.M. 2017 Effect of wall cooling on boundary-layer-induced pressure fluctuations at Mach 6. *J. Fluid Mech.* **822**, 5–30.
ZHANG, C., DUAN, L. & CHOUDHARI, M.M. 2018 Direct numerical simulation database for supersonic and hypersonic turbulent boundary layers. *AIAA J.* **56** (11), 4297–4311.
ZHANG, P.-J.-Y., WAN, Z.-H., LIU, N.-S., SUN, D.-J. & LU, X.-Y. 2022 Wall-cooling effects on pressure fluctuations in compressible turbulent boundary layers from subsonic to hypersonic regimes. *J. Fluid Mech.* **946**, A14.
ZHANG, P.-J.-Y., WAN, Z.-H., SUN, D.-J. & LU, X.-Y. 2024 The intrinsic scaling relation between pressure fluctuations and Mach number in compressible turbulent boundary layers. *J. Fluid Mech.* **993**, A2.
ZHANG, Y.-S., BI, W.-T., HUSSAIN, F. & SHE, Z.-S. 2014 A generalized Reynolds analogy for compressible wall-bounded turbulent flows. *J. Fluid Mech.* **739**, 392–420.